Acta Pharmaceutica Sinica B 2026;16(3):1773−1778

Chinese Pharmaceutical Association
Institute of Materia Medica, Chinese Academy of Medical Sciences

Acta Pharmaceutica Sinica B

www.elsevier.com/locate/apsb
www.sciencedirect.com

LETTER TO THE EDITOR

Multi-omics-based identification of METTL11B as a novel biomarker in esophageal squamous cell carcinoma

KEY WORDS

Esophageal squamous cell carcinoma;
Molecular profile;
Biomarkers;
Regulatory network;
Drug target;
Precision medicine

To the Editor:

Esophageal cancer, the seventh most lethal cancer in the world, is divided into two pathologically distinct subtypes: esophageal squamous cell carcinoma (ESCC; accounts for over 90%) and esophageal adenocarcinoma, which differ significantly in risk and geographic factors[1,2]. The major geographic prevalence of ESCC is in East Asia, with China accounting for more than half of all cases worldwide[3]. Despite advances in diagnostic and therapeutic modalities, the five-year overall survival for ESCC patients remains dismal (<30%), primarily due to the paucity of robust biomarkers for early detection and precision medicine[4,5]. Therefore, gaining deeper insights into the molecular profile of ESCC and identifying novel ESCC biomarkers will facilitate accurate diagnosis and effective treatment[6]. Herein, we carried out a comprehensive transcriptomics analysis of tissue samples from 50 cases of ESCC patients, characterizing mRNA expression features in tumor tissues versus their paired non-cancerous adjacent tissues. By constructing a molecular co-expression network and locating the core network, a group of potential biomarkers of ESCC was found. In addition, to avoid the limitations of one-dimensional omics, we integrated The Cancer Genome Atlas (TCGA)-ESCC gene expression and copy number variation multi-omics data to classify patients and observe the clinical outcome of each subgroup. Through the above analysis, we revealed methyltransferase-like protein 11B (*METTL11B*; also known as *NTMT2*) as a potential biomarker for ESCC, which is essential for the proliferative and migratory capacities of ESCC cells. Finally, knockdown of *METTL11B* restored the level of retinoblastoma-associated protein (RB1), a tumor suppressor protein and a reported methylation substrate for *METTL11B*, probably through heightening RB1 protein stability.

1. Identification of *METTL11B* as a novel biomarker for ESCC

In this study, we collected tumor tissues from 50 ESCC patients and their paired adjacent non-cancerous tissues for RNA-seq (Supporting Information Fig. S1). We used Trim Galore to clean and control the raw data from the disembarked machine, and Kallisto to compare and quantify transcript expression levels, followed by downstream bioinformatic analysis (Fig. 1A; Supporting Information Tables S1 and S2). Satisfactory sequencing depth and data quality were observed in our transcriptome data, with RAW_READS across all samples over 20 M, RawQ30 over 85%, and Mapped over 80%. Through principal components analysis, we revealed considerable separation of tumor and non-cancerous adjacent tissues with apparently distinct mRNA expression features in the progression of ESCC, which also demonstrated a good quality for our clinical samples (Supporting Information Fig. S2A). First, we utilized the gene set enrichment analysis (GSEA) to interrogate pathway anomalies within the tumor landscape and discovered that cell cycle-related genes altered dramatically as ESCC progressed, which is consistent with earlier findings[7,8] (Fig. S2B). Subsequently, we investigated the difference in the expression levels between these two groups and discovered that, compared to non-cancerous adjacent tissues,

Peer review under the responsibility of Chinese Pharmaceutical Association and Institute of Materia Medica, Chinese Academy of Medical Sciences.

https://doi.org/10.1016/j.apsb.2026.01.025

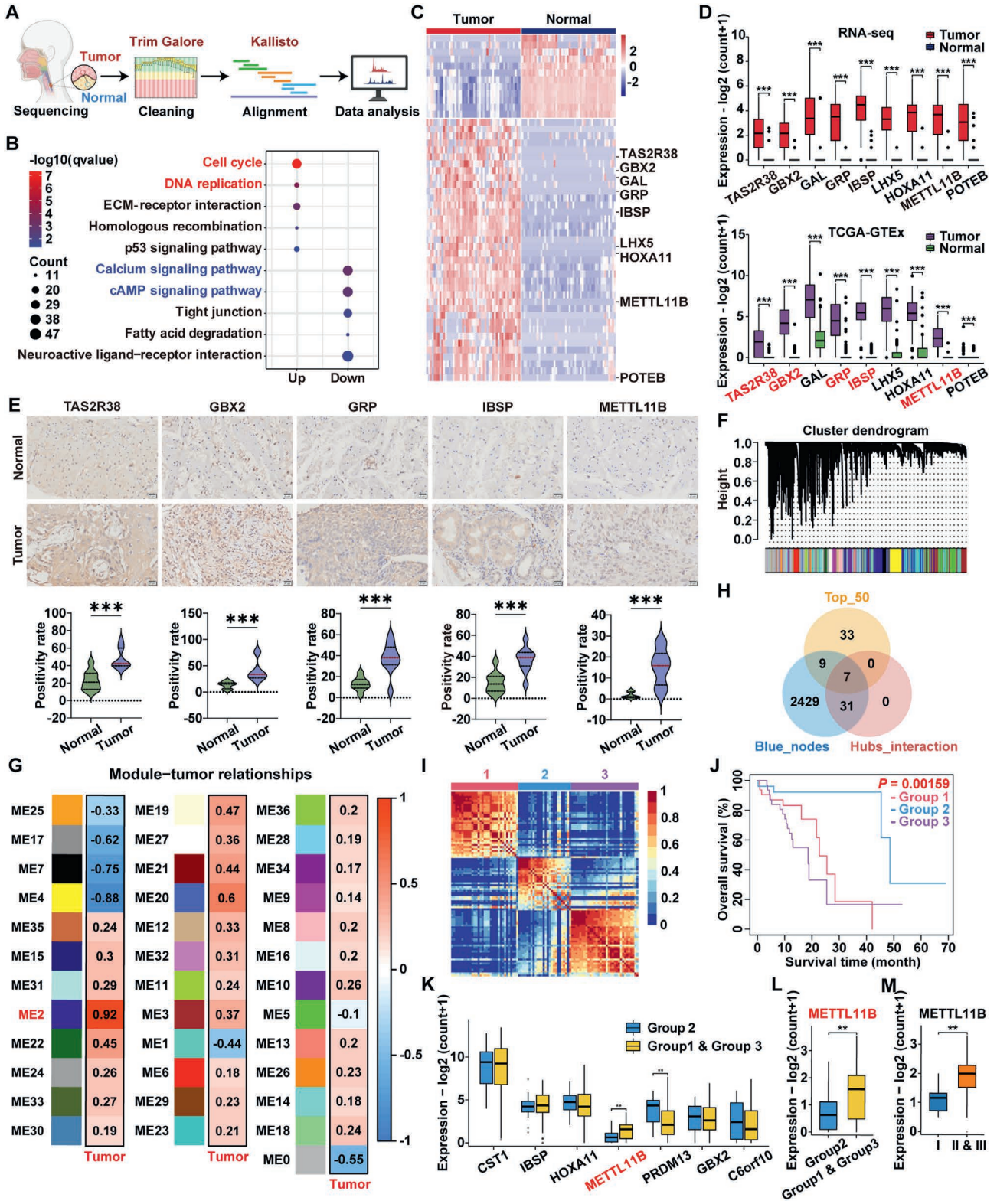

Figure 1 Identification of novel biomarkers for esophageal squamous cell carcinoma (ESCC). (A) The pipeline of the upstream data processing. (B) Bubble plot of Kyoto Encyclopedia of Genes and Genomes pathways enriched by the significantly up-regulated and down-regulated genes in the tumor compared with non-cancerous adjacent tissues. (C) Heat map of the top 50 significantly differentially expressed genes. (D) Box plots of different expression of 9 genes in tumor and non-cancerous adjacent tissues in our sequencing data and the public The Cancer Genome Atlas and GTEx data, respectively. (E) Representative images of immunohistochemical staining of five markers expressed in ESCC tissue and normal tissue ($n = 10$). Scale bar, 20 μm. Compared with the normal tissue, $^{***}P < 0.001$. (F) Clustering dendrogram of genes in each module. (G) Heatmap of correlation between eigengenes of each module and tumor trait. (H) Venn plot of the top 50 significantly differentially expressed

the expression levels of 3490 genes in tumor tissues were significantly altered, with 1595 genes up-regulated and 1895 genes down-regulated ($P_{adj} < 0.05$ and $|\log_2 \text{Foldchange}| > 1$; Fig. S2C). Subsequent Kyoto Encyclopedia of Genes and Genomes pathway analysis of the differentially expressed genes revealed that up-regulated genes were significantly enriched in cell cycle processes (consistent with our GSEA findings) and DNA replication. Conversely, down-regulated genes were primarily associated with calcium and cAMP signaling cascades (Fig. 1B; Fig. S2D). Among the top 50 genes with most obviously changed expression, *TAS2R38*, *GBX2*, *GAL*, *GRP*, *IBSP*, *LHX5*, *HOXA11*, *METTL11B*, and *POTEB* were only expressed in tumors (Fig. 1C and D). Notably, *TAS2R38*, *GBX2*, *GRP*, *IBSP*, and *METTL11B* were further shown to be expressed only in tumors in the TCGA-ESCC cohort and the GTEx database. As a result, we speculate that these five genes were intimately linked to the ESCC tumorigenesis and would prioritize them for downstream investigation (Fig. 1D). Through immunohistochemical analysis, we found that in 10 pair clinical samples, all five markers were highly expressed in ESCC samples compared to normal tissues, indicating the potential for targeted treatment of ESCC (Fig. 1E). We then collected clinical traits of 50 pairs samples, and subjected our RNA-seq data to weighted correlation network analysis (Supporting Information Fig. S3). Sample dendrogram and trait heatmap also showed that we sampled well (Fig. S3A). We discovered that the scale-free topology fitting index R^2 first surpasses 0.9, and the mean connectivity has fallen below 100 when the soft threshold is 9 (Fig. S3B; Supporting Information Table S3). To get the network closer to the scale-free distribution, we utilized 9 as the soft threshold to calculate the weighted correlation between genes and created the adjacency matrix to generate the systematic clustering tree between genes. The gene modules were then sliced using a hybrid dynamic shear tree, clustered, and merged again. A total of 37 gene clusters with comparable expression patterns were found (Fig. 1F). Subsequently, we correlated the genes in the modules with clinical traits, and found that the blue module had the strongest association with the tumor group (Fig. S3C; Supporting Information Fig. S4A and S4B). Notably, the correlation between the blue module and the tumor was 0.92 ($P < 0.001$; Fig. 1G). We calculated the module membership (MM) with the blue module, and gene significance (GS) with the tumor of each gene, and obtained 299 hub genes highly associated with both the blue module ($|\text{MM}| > 0.8$) and tumor ($|\text{GS}| > 0.2$; Supporting Information Table S4). Unsurprisingly, the correlation between blue MM and GS was 0.91 ($P < 0.001$), indicating the pivotal role of blue module genes in the pathogenesis and progression of ESCC (Fig. S4C). Subsequently, we further found that the blue module contained 16 differentially expressed genes of the top 50, of which 7 genes could regulate a certain number of hub genes in the blue module, and we regarded these 7 genes as ESCC candidate biomarkers (Fig. 1H). Notably, all of *GBX2*, *IBSP*, and *METTL11B* appeared in five genes that are only expressed in tumors, indicating their dual value as both specific biomarkers and mechanistic drivers. In addition, to avoid the limitations of one-dimensional omics, we integrated TCGA-ESCC gene expression and copy number variation multi-omics data to classify patients and observe the clinical outcomes of each subgroup[9]. The consensus matrix showed that patients could be stably divided into three subgroups with different molecular characteristics (Supporting Information Fig. S4D). We combined the consensus clustering and similarity network fusion methods to divide patients into three subgroups with different molecular characteristics, namely group 1 ($n = 33$), group 2 ($n = 26$), and group 3 ($n = 33$; Fig. 1I). Among them, patients in group 2 had a better outcome than patients in groups 1 and 3 ($P = 0.00159$; Fig. 1J). We further evaluated the expression of 7 candidate ESCC biomarkers in group 2 and group 1 plus 3, and found that *METTL11B* and *PRDM13* showed significant differences between these groups (Fig. 1K). We found that the number of hub genes in the blue module connected by *METTL11B* is much higher than that for *PRDM13*, hinting that *METTL11B* is more relevant to ESCC progression (Supporting Information Fig. S5A). Collectively, our comprehensive evaluation established *METTL11B* as a novel ESCC biomarker with robust diagnostic specificity, therapeutic centrality, and clinical prognostic value (Fig. S5B). Indeed, patients in group 2 generally have a lower level of *METTL11B* expression (Fig. 1L). In addition, our sequencing data revealed a positive correlation between elevated *METTL11B* expression and advanced tumor stages (Fig. 1M). *METTL11B* connects 118 hub genes in the ESCC-related network, but, strikingly, its aberrant expression was not reported previously for ESCC (Fig. S5A). Therefore, it is reasonable to infer that *METTL11B* intervention is likely to trigger changes in the hub gene network, intimately associated with the occurrence and progression of ESCC.

2. *METTL11B* promotes ESCC progression

Notably, we utilized the ESCC tissue microarray to evaluate clinical relevance and found METTL11B expression was higher in 56 ESCC tissues than in corresponding normal tissues, with a significant difference (Fig. 2A; Supporting Information Fig. S6A). Given the elevated expression of *METTL11B* in ESCC, we selected TE-1 and ECA-109 cell lines, which exhibited relatively high *METTL11B* expression among ESCC cell lines, for further exploration (Supporting Information Fig. S7A). We first measured ESCC cell proliferation after *METTL11B* knockdown (Fig. 2B; Fig. S6B) by MTT assay and colony formation assay. We revealed that *METTL11B* knockdown significantly reduced proliferation in TE-1 and ECA-109 cells (Fig. 2C and D; Fig. S6C). Further, we employed sequencing data to calculate the correlation between all genes and *METTL11B*, followed by GSEA analysis, and revealed that *METTL11B* was substantially linked with epithelial-mesenchymal transition (Fig. 2E). GSEA analyses observed similar results by comparing the groups with high or low *METTL11B* expression (Fig. S7B and S7C). Indeed, cell migration was notably impaired in the sh-*METTL11B*-treated group versus the negative control (NC) group (Fig. 2F; Fig. S6D). qPCR

genes in our sequencing data, blue module genes, and genes that interact with hub genes. (I) Heatmap of patient similarity matrix identified by consensus clustering combined with similarity network fusion. (J) Overall survival curves for the three subgroups. (K) Box plots of the expression of ESCC candidate biomarkers in group 2 and group 1 plus 3. (L) Box plots of methyltransferase-like protein 11B (*METTL11B*) expression in group 2 and group 1 plus 3. (M) Box plots of *METTL11B* expression at stage I and II plus III patients in our sequencing data. $^{**}P < 0.01$.

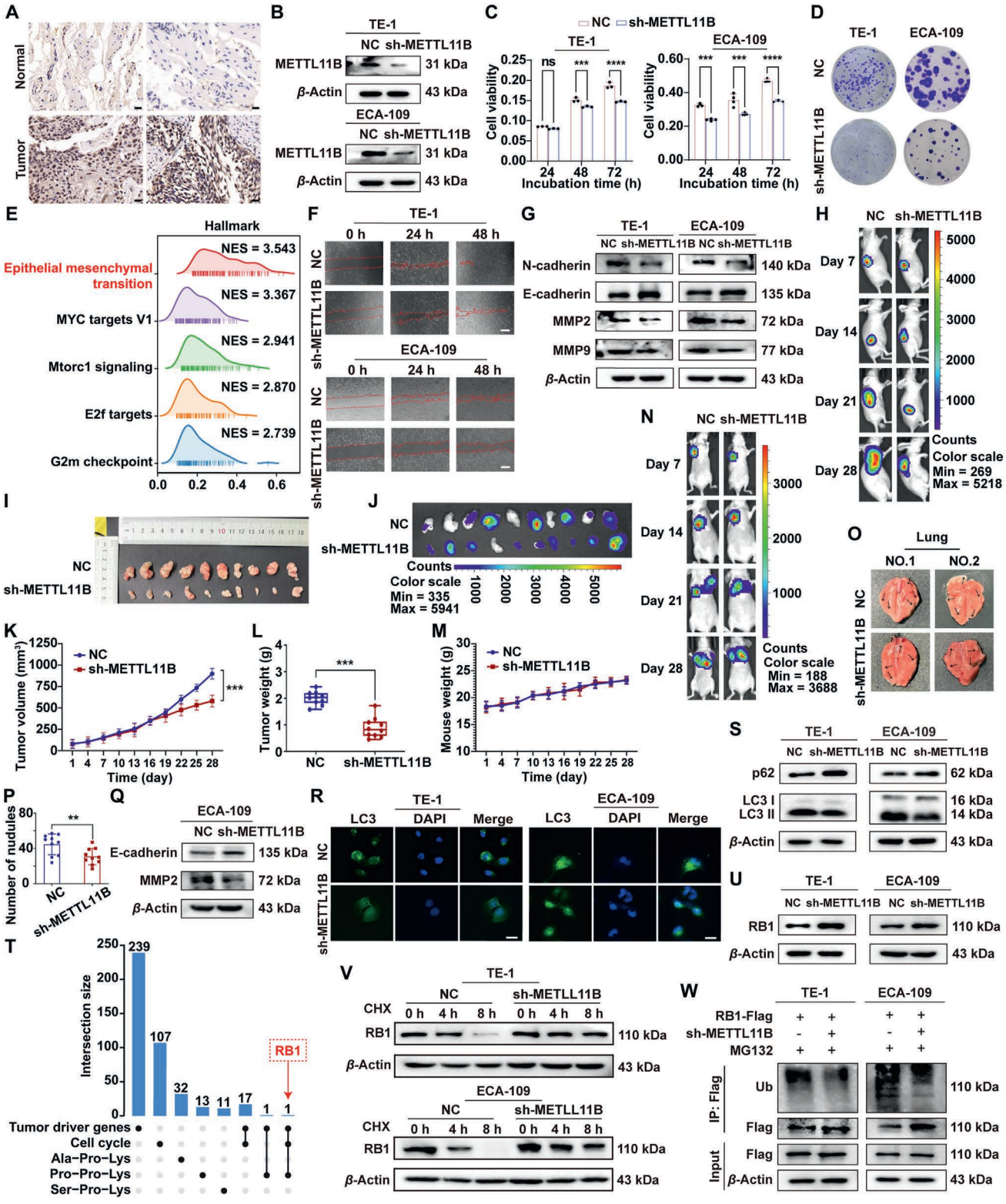

Figure 2 *METTL11B* promotes ESCC progression. (A) Representative immunohistochemical staining of METTL11B expression in ESCC and paired normal tissues ($n = 56$). Scale bar, 20 μm. (B) The knockdown efficiency of *METTL11B* in TE-1 and ECA-109 was verified by Western blot assay. (C) MTT assay assessing cell proliferation following *METTL11B* knockdown. ns, not significant, $^{***}P < 0.001$, $^{****}P < 0.0001$ compared with the control groups. (D) Colony formation assay evaluating long-term proliferation capabilities following *METTL11B* knockdown. (E) Mountain plot of gene set enrichment analysis of *METTL11B*. (F) Scratch assay assessing cell migration after knockdown of *METTL11B*. Scale bar, 100 μm. (G) Western blot assay showing that the knockdown of *METTL11B* in TE-1 and ECA-109 caused a reduction in cell metastasis. (H) *In vivo* bioluminescence imaging of the subcutaneous xenograft model from the NC group and the *sh-METTL11B* group. (I) Representative

experiments showed that the sh-*METTL11B* group had lower N-cadherin, *MMP2*, and *MMP9* expression and higher E-cadherin expression (Fig. S7D). Consistently, Western blot analysis showed that *METTL11B* knockdown increased E-cadherin expression with reduced levels for N-cadherin, MMP2, and MMP9, suggesting a regulatory role of *METTL11B* on epithelial-mesenchymal transition markers (Fig. 2G; Fig. S6E). To validate the oncogenic function of *METTL11B in vivo*, we established a subcutaneous xenograft model by inoculating ECA-109-luc cells into nude mice. Comprehensive assessment *via* bioluminescence imaging, tumor volume, and weight measurements revealed that *METTL11B* knockdown significantly attenuated tumor progression compared to the NC-group, which saline-treated tumors (Fig. 2H−L). Importantly, no behavioral abnormalities or significant weight loss were observed in the treatment group, indicating a lack of systemic toxicity (Fig. 2M). These findings collectively confirm that *METTL11B* depletion suppresses ESCC tumorigenicity *in vivo.* To further evaluate the metastatic potential, we employed a tail vein injection nude mouse model. Bioluminescence tracking and pulmonary nodule quantification demonstrated that METTL11B knockdown markedly inhibited lung colonization and metastasis (Fig. 2N−P). Mechanistically, lung tissues from the *sh-METTL11B* group exhibited downregulated MMP2 and upregulated E-cadherin levels, corroborating the suppression of the metastatic phenotype (Fig. 2Q; Fig. S6F). Several recent studies have shown that consolidating autophagy promotes ESCC progression and leads to resistance to radiotherapy and chemotherapy[10,11]. Immunofluorescence analysis of LC3 confirmed that the intensity of the LC3 signal was significantly lower in the sh-*METTL11B* group than that in the NC group, indicating that autophagy was inhibited following *METTL11B* knockdown (Fig. 2R; Fig. S6G). We also observed an increase in p62 and a decrease in the LC3 II/LC3 I ratio in *METTL11B*-knockdown cells (Fig. 2S; Fig. S6H). These functional validations demonstrated that loss of *METTL11B* inhibited ESCC cell proliferation, migration, and autophagy. METTL11B is an alpha *N*-methyltransferase[12]. To further explore the mechanism underlying METTL11B's regulatory role in tumorigenesis, we screened potential METTL11B substrates containing a reported N-terminal motif Ala/Pro/Ser-Pro-Lys[12], and found that two of these substrates are tumor-related genes (Fig. 2T; Supporting Information Table S5). Of our particular interest, RB1 protein is a tumor suppressor that binds E2F transcription factors and prevents transcription of its downstream genes in its hypophosphorylated state[13]. Notably, RB1 functions as a cell cycle modulator[13], hinting at its potential involvement in the abnormal cell-cycle regulation in ESCC shown by our omics analyses (Fig. 1B; Fig. S2B). Interestingly, *METTL11B* knockdown increased both the cellular abundance and the half-life of RB1 protein without affecting its mRNA level (Fig. 2U and V, Fig. S6I and S6J, Supporting Information Fig. S8A). In addition, expression of *METTL11B* and *RB1* was not correlated in the RNA-seq results (Fig. S8B and S8C), suggesting that *METTL11B* regulates RB1 expression, probably by governing its protein stability. We further conducted relevant experiments to clarify whether regulating *METTL11B* affects the ubiquitination of RB1. Reduced RB1 ubiquitination in the sh-*METTL11B* group was observed compared to the NC group, supporting the hypothesis that *METTL11B* destabilizes RB1 through N-terminal methylation and promotes the degradation of RB1 through the ubiquitin-proteasome degradation (Fig. 2W). In conclusion, our findings unveil METTL11B as a previously unrecognized biomarker that is significantly overexpressed in ESCC and critical for tumor advancement. Moreover, our findings demonstrate that *METTL11B* is functionally associated with ESCC cell phenotype, including proliferation, migration, and autophagy induction, and experimentally validated to drive tumor growth and metastasis *in vivo*, underscoring the potential of *METTL11B* as a candidate for targeted intervention in ESCC.

Acknowledgments

This work was supported by Chengdu Science and Technology Bureau Program (Grant No. 2024-YF05-00448-SN; Yong Yuan, China). This work was supported by the National Natural Science Foundation of China (Grant No. 82373764; Ning Li). This work was supported by Sichuan Science and Technology Program (Grant No. 2023NSFSC1924; Rui Liu, China), and the Research and Develop Program, West China Hospital of Stomatology Sichuan University (Grant No. RD-03-202404; Rui Liu, China).

Author contributions

Wenke Jin: Conceptualization, Investigation, Formal analysis, Visualization, Data curation; Writing - original draft. Hongyao Li: Investigation, Formal analysis, Writing - original draft. Yanmei Chen: Investigation, Formal analysis, Writing - original draft. Wei Wang: Conceptualization, Writing - review & editing, Supervision. Rui Liu: Conceptualization, Writing - review & editing, Supervision, Funding acquisition. Ning Li: Conceptualization, Writing - review & editing, Supervision, Funding acquisition. Yong Yuan: Conceptualization, Writing - review & editing, Supervision, Funding acquisition.

images of excised xenograft tumors. (J) *Ex vivo* fluorescence imaging of tumors after the intraperitoneal injection of fluorescein potassium salt. Scale bar, 0.5 cm. (K) Quantitative analysis of the ECA-109-luc cells tumor volume. (L) Quantitative analysis of the ECA-109-luc cell tumor weight. (M) Quantitative analysis of the ECA-109-luc cells induced mouse weight. (N) Bioluminescence imaging of the tail vein metastasis mode. (O) Representative images of lung metastasis from nude mice. The arrow represents a pulmonary metastatic nodule. (P) Quantification of pulmonary metastatic nodules in nude mice. $^{**}P < 0.01$ compared with the control groups. (Q) Western blot analysis of E-cadherin and MMP2 expression in lung tissues from the NC and sh-*METTL11B* group nude mice. (R) The effect of knockdown of *METTL11B* on autophagy in TE-1 and ECA-109 cells was detected by LC3 immunofluorescence assay. Scale bar, 10 μm. (S) Western blot analysis showing that the knockdown of *METTL11B* in TE-1 and ECA-109 resulted in diminished cellular autophagy. (T) Upset plot of genes containing N-terminal motif Ala/Pro/Ser-Pro-Lys, tumor driver genes, and cell cycle-related genes. Tumor driver genes were summarized by Bailey et al.[14]. (U) The expression of retinoblastoma-associated protein (RB1) after knockdown of *METTL11B* in TE-1 and ECA-109 cell lines was detected by Western blot assay. (V) The effect of *METTL11B* knockdown in TE-1 and ECA-109 cell lines on RB1 degradation was analyzed by Western blot after administration of CHX (100 μg/mL) to block protein synthesis for 0, 4, and 8 h. (W) Flag-RB1 was transfected into TE-1 and ECA-109 cell lines, and the ubiquitination level of RB1 in the cells was analyzed by Western blot. The cells were pretreated with 10 μmol/L MG132 for 6 h before harvest.

Conflicts of interest

The authors have declared that no competing interest exists.

Appendix A. Supporting information

Supporting information to this article can be found online at https://doi.org/10.1016/j.apsb.2026.01.025.

References

1. Bray F, Laversanne M, Sung H, Ferlay J, Siegel RL, Soerjomataram I, et al. Global cancer statistics 2022: GLOBOCAN estimates of incidence and mortality worldwide for 36 cancers in 185 countries. *CA Cancer J Clin* 2024;**74**:229−63.
2. Smyth EC, Lagergren J, Fitzgerald RC, Lordick F, Shah MA, Lagergren P, et al. Oesophageal cancer. *Nat Rev Dis Primers* 2017;**3**: 17048.
3. Ferlay J, Ervik M, Lam F, Laversanne M, Colombet M, Mery L, et al. *Global cancer observatory: cancer today.* Lyon, France: International Agency for Research on Cancer; 2024. Available from: https://gco.iarc.who.int/today. [Accessed 24 October 2024].
4. He S, Xu J, Liu X, Zhen Y. Advances and challenges in the treatment of esophageal cancer. *Acta Pharm Sin B* 2021;**11**:3379−92.
5. Zhang X, Peng L, Luo Y, Zhang S, Pu Y, Chen Y, et al. Dissecting esophageal squamous-cell carcinoma ecosystem by single-cell transcriptomic analysis. *Nat Commun* 2021;**12**:5291.
6. Zhang X, Wang Y, Meng L. Comparative genomic analysis of esophageal squamous cell carcinoma and adenocarcinoma: new opportunities towards molecularly targeted therapy. *Acta Pharm Sin B* 2022;**12**:1054−67.
7. Cancer Genome Atlas Research Network. Integrated genomic characterization of oesophageal carcinoma. et al. *Nature* 2017;**541**: 169−75.
8. Cui Y, Chen H, Xi R, Cui H, Zhao Y, Xu E, et al. Whole-genome sequencing of 508 patients identifies key molecular features associated with poor prognosis in esophageal squamous cell carcinoma. *Cell Res* 2020;**30**:902−13.
9. Zhang S, Zhang J, An Y, Zeng X, Qin Z, Zhao Y, et al. Multi-omics approaches identify SF3B3 and SIRT3 as candidate autophagic regulators and druggable targets in invasive breast carcinoma. *Acta Pharm Sin B* 2021;**11**:1227−45.
10. Khan T, Relitti N, Brindisi M, Magnano S, Zisterer D, Gemma S, et al. Autophagy modulators for the treatment of oral and esophageal squamous cell carcinomas. *Med Res Rev* 2020;**40**:1002−60.
11. Liu Y, Wang Y, Zhang J, Peng Q, Wang X, Xiao X, et al. Nanotherapeutics targeting autophagy regulation for improved cancer therapy. *Acta Pharm Sin B* 2024;**14**:2447−74.
12. Tooley CE, Petkowski JJ, Muratore-Schroeder TL, Balsbaugh JL, Shabanowitz J, Sabat M, et al. NRMT is an alpha-N-methyltransferase that methylates RCC1 and retinoblastoma protein. *Nature* 2010;**466**: 1125−8.
13. Harbour JW, Luo RX, Dei Santi A, Postigo AA, Dean DC. Cdk phosphorylation triggers sequential intramolecular interactions that progressively block Rb functions as cells move through G1. *Cell* 1999; **98**:859−69.
14. Bailey MH, Tokheim C, Porta-Pardo E, Sengupta S, Bertrand D, Weerasinghe A, et al. Comprehensive characterization of cancer driver genes and mutations. *Cell* 2018;**173**:371-85.e18.

Wenke Jin[a,b,c,†], Hongyao Li[a,†], Yanmei Chen[a,†], Wei Wang[d,e,*], Rui Liu[c,*], Ning Li[b,*], Yong Yuan[a,*]

[a]*Department of Thoracic Surgery, Med+X Center for Informatics, West China Hospital, Sichuan University, Chengdu 610041, China*
[b]*School of Traditional Chinese Materia Medica, Key Laboratory of Innovative Traditional Chinese Medicine for Major Chronic Diseases of Liaoning Province, Key Laboratory for TCM Material Basis Study and Innovative Drug Development of Shenyang City, Shenyang Pharmaceutical University, Shenyang 110016, China*
[c]*State Key Laboratory of Oral Diseases & National Center for Stomatology & National Clinical Research Center for Oral Diseases & Chinese Academy of Medical Sciences Research Unit of Oral Carcinogenesis and Management, Department of Oral Medicine, West China Hospital of Stomatology, Sichuan University, Chengdu 610041, China*
[d]*Department of Thoracic Surgery, Liaoning Cancer Hospital & Institute, Cancer Hospital of China Medical University, Shenyang 110042, China*
[e]*Department of Thoracic Surgery, Cancer Hospital of Dalian University of Technology, Liaoning Cancer Hospital & Institute, Shenyang 110042, China*

*Corresponding authors.
E-mail addresses: yongyuan@scu.edu.cn (Yong Yuan), liningsypharm@163.com (Ning Li), liurui_scu@hotmail.com (Rui Liu), wangwei_9111@hotmail.com (Wei Wang)

[†]These authors made equal contributions to this work.

Received 12 August 2025
Received in revised form 12 November 2025
Accepted 13 November 2025